Extended Dynamics of the Remarkable Dynabee

Gregory W. Ojakangas[*]

Department of Chemistry and Physics, Drury University

900 N Benton Ave, Springfield, MO, 65802

email: gojakang@drury.edu

ABSTRACT

The dynabee is a remarkable hand-held invention which accelerates an enclosed gyroscopic rotor to high spin rates by manipulating its axle ends within an enclosure shaped like the inside of a tire – comprising upper and lower opposing tracks. When the rotor possesses adequate angular momentum, and the enclosure is properly manipulated by the user, the axle ends can slide continuously against opposing tracks, with concommitant acceleration of the rotor's spin, through friction between the axle ends and the tracks. Sliding friction is responsible for the acceleration, through the intermediate agent of the Coriolis force. We examine the mechanics of the device in the most complete and realistic manner to date, using two coupled differential equations describing (respectively) the rotation rate of the rotor and the rate at which its axis precesses about the enclosure. The latter variable behaves as a damped pendulum when capture of the system into resonance occurs. By including the effects of gravitational acceleration on the system, the minimum axial spin rate that allows rotor acceleration is found. The dynamics of the dynabee provide a visceral analog to the mechanisms underlying the common synchronous rotation states of nearly all moons in the solar system, and they serve as a delightful pedagogical illustration of how capture probability is relevant in a classical dynamical system.

I. INTRODUCTION: THE MECHANISM OF ACCELERATION

The gyroscopic wrist exercising device originally known as the Dynabee[1], also called the Force Ball, or the Roller Ball, utilizes a unique mechanism to accelerate an enclosed, roughly spherical rotor to high rotation rates – each end of the rotor's axle slides while rolling along opposing insides of an enclosed track (Fig.1) , accelerated by the friction torques supplied at these contacts.[2] A guide ring (not shown), piercing both ends of the axle, keeps the
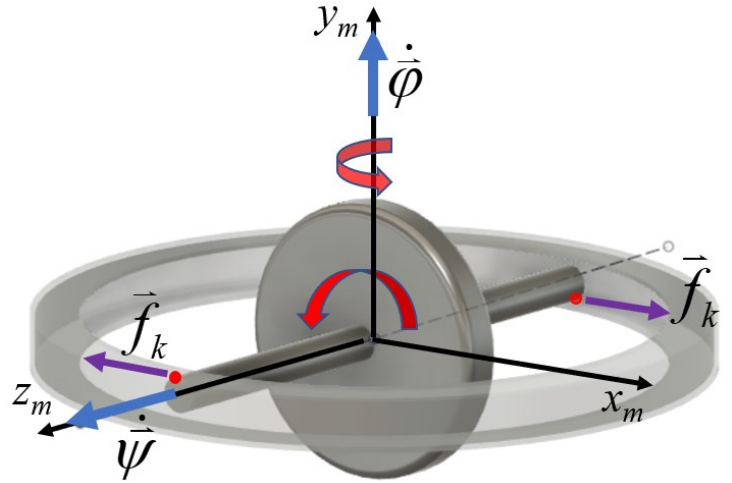

Fig. 1 Schematic of dynabee. Actual rotor is nearly spherical. Dots on axle ends indicate points of sliding contact between axle and tracks. Friction forces $\vec{f}_k$ acting on the axle ends are shown for the case where $\dot{\psi} < \zeta\dot{\varphi}$, wherein sliding accelerates the rotor's axial spin $\dot{\psi}$. Axes of the important "model coordinate system" are also shown.

rotor centered. Once the rotor is given an adequate initial axial spin, appropriate manipulation of the housing leads to its acceleration, while the rotor axle simultaneously precesses about the track. It is easy to see that if both ends of the axle were to slide on the same surface (say, the lower one in Fig.1) while precessing, the two friction torque components along the rotor's symmetry axis would cancel each other out. However, something remarkable happens when each axle end slides on an *opposing* track. The sliding friction torques add together, with a resultant twice as great in magnitude as either individually! This is marvelous, as it represents a novel way to accelerate a gyroscopic rotor. With the nonzero torque, the spin must either accelerate or decelerate, and it turns out that the acceleration's sign depends straightforwardly on the value of the axial spin $\dot{\psi}$ relative to the rate of precession $\dot{\varphi}$.

To see this dependence, first note that during increases $\Delta\varphi$ and $\Delta\psi$ in the precession and axial rotation angles, the axle's contacts with the surface cover distances $R_A\Delta\psi$ relative to the rotor

and $R_T\Delta\varphi$ relative to the track, where R_A and R_T are the axle and track radii. These distances are the same when there is no slipping: $R_A\Delta\psi = R_T\Delta\varphi$, in other words $\dot\psi = \varsigma\dot\varphi$, where $\varsigma \equiv R_T/R_A$. It follows that if $\dot\psi \neq \varsigma\dot\varphi$ the axle will slide while rolling, but in what direction? Fig.1 depicts the situation when $\dot\psi < \varsigma\dot\varphi$, corresponding to a slowly spinning axle, in which case both kinetic friction forces generate torques which are seen to spin up the rotor. The torque reverses sign when $\dot\psi > \varsigma\dot\varphi$, and the rotor decelerates.

Synchronization of the frequency of manipulation of the housing with that of the precession is also critical to the acceleration process. Heyda[3] relates motion of the rotor to the torque supplied by the user, without directly addressing the intermediate agent of friction. Gulick and O'Reilly[4] describe the kinetics of this device in the most complete manner prior to this work, but they only considered static friction (rolling without slipping). Therefore the ratio of axial spin to precession rate of the rotor's symmetry axis is assumed in [4] to be precisely equal to ζ. It is clear, however, that *sliding* friction is the critically important process that accelerates the rotor, since the mechanism of initiating the desired motion involves rapid acceleration of the rotor's spin (e.g. by dragging the exposed part of the rotor against a frictional surface), followed by a sudden tilt of the housing, such that the axle ends begin to slide immediately against the track. Herein we examine equations of motion for the system in the case of sliding friction and gravity.

[3] and [4] describe different methods of accelerating the rotor, both of which are typically discovered by users as they learn to use the device. [3] adopts the simplest method, which involves rocking the housing back and forth with simple harmonic motion about a fixed horizontal axis. When the rocking frequency coincides with that of axial precession, with a suitable phase lag, acceleration of the rotor occurs. [4] describes a more effective method of manipulating the

housing, which we also adopt (Section II). The method in [3] is simpler to perform, but less efficient at accelerating the rotor.

II.   COORDINATE SYSTEMS AND KINEMATIC VARIABLES

The housing contains two opposing circular tracks, like the inside of a tire. When in operation, the two axle ends are in contact with opposite surfaces. An inertial coordinate system (x_I, y_I, z_I) is defined such that the z_I-axis is in the vertical direction, opposite to gravity, with the origin at the center of the track (Fig.2a). We use a ZXZ Euler rotation sequence[5] to transform from the
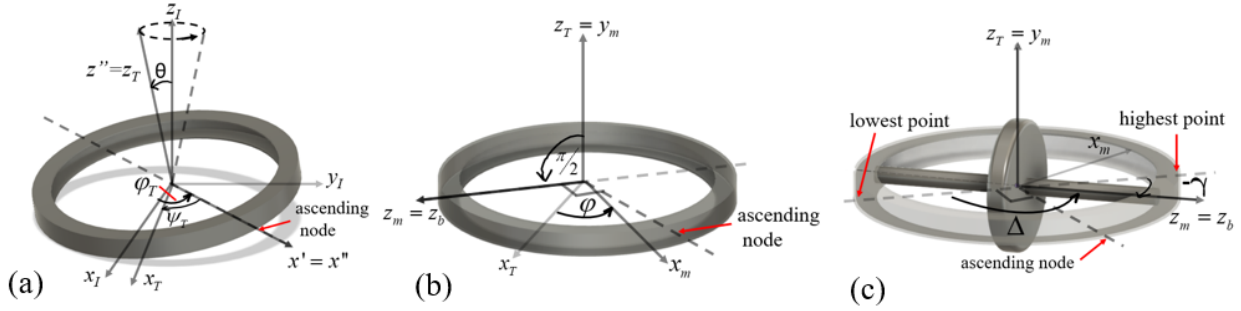

Fig.2 (a) sequential ZXZ Euler rotations by φ_T, θ, and ψ_T effect the transformation from inertial space to the track coordinate system. Note that $\varphi_T = -\psi_T$. (b) sequential ZX Euler rotations by φ and $\pi/2$ transform from the track to the model coordinate system, and a final Z-axis rotation leads to the body coordinate system (not shown). (c) typical approximate equilibrium orientation where the angle $\Delta \equiv \varphi - \varphi_T$. Note that the $+z_b$-axis leads the ascending node of the (x_T, y_T)-plane on the (x_I, y_I)-plane.

inertial coordinate system to the coordinates fixed to the track, which are denoted by (x_T, y_T, z_T). This involves sequential rotations by φ_T, θ, and ψ_T about the z_I-axis, the resulting x' axis, and the resulting z'' axis, respectively. Following [4] we prescribe θ as a constant, and (importantly) that $\psi_T = - \varphi_T$. If φ_T increases at a constant rate, this peculiar prescription leads to motion of the housing that superficially resembles the wobbling of a coin on a tabletop – notably with the z_T-axis precessing about the vertical inertial axis, with constant coning angle θ (Fig.2a). The phase of this wobbling motion can be followed using the line of intersection between the (x_T,y_T)-plane

and the (x_I, y_I)-plane (i.e. the nodal line of the (x_T, y_T)-plane relative to the inertial coordinate system) which precesses about the z_I-axis as φ_T increases. Notably, the track undergoes no net rotation once φ_T completes a full cycle – the housing is back where it started. For visualization of the prescribed motion of the housing, it helps to note that φ_T is equal to the longitude of the ascending node of the (x_T, y_T)-plane, as measured in the inertial coordinate system.

Having prescribed the track's motion relative to inertial space, we now seek to describe the motion of the rotor relative to the track. For simplicity, we assume that the diameter of the axle ends is negligibly smaller than the separation between the lower and upper tracks, so the axis of the rotor lies within the $\left(x_T, y_T \right)$-plane. From the track coordinate system, we employ another ZXZ Euler rotation sequence (see Fig.2b), rotating by φ about the z_T axis, then by $\pi/2$ about the resulting x-axis, thus arriving at the *model coordinate system*, with coordinates denoted by (x_m, y_m, z_m). The third Euler rotation, by ψ about the z_m axis, leads to the *body* coordinate system defined by (x_b, y_b, z_b). The z_m axis is coincident with the z_b axis (i.e. parallel to the axle of the rotor), the y_m axis is parallel to the z_T axis, and the x_m axis lies in the plane of the track. We further prescribe that the $+z_b$-end of the axle rotates counterclockwise ($\dot{\psi} > 0$), while precessing counterclockwise ($\dot{\varphi} > 0$) about the y_m-axis (as in Fig.1). This motion requires the $+z_b$ – end of the axle to be pressed against the *upper* track surface. Note that the *model* coordinate system does not rotate with the rotor, but remains coincident with the figure of the axisymmetric rotor, while it precesses with the z_b-axis about the track (Fig.2c).

We now define a new variable

$$\Delta \equiv \varphi - \varphi_T \qquad (1)$$

and we replace φ by $\Delta + \varphi_T$ wherever it appears. Note that if $\Delta = 0$, so that $\varphi = \varphi_T$, then the $+ z_b$

axis lags the ascending node by $\pi/2$, and points toward the track's lowest point in the inertial z -

coordinate. Therefore Δ may be identified with the angular position of the positive z_b axis on the

(x_T, y_T)-plane, relative to the point of lowest geographical altitude. Also note that if $\Delta = \pi$, the

same axis is at the highest altitude. We show below that during normal operation of the device,

the axle behaves as a damped pendulum, oscillating about a position close to $\Delta = \pi$. This

equilibrium position of the rotor's spinning figure is depicted approximately in Fig (2c).

III.   FICTITIOUS TORQUES IN THE MODEL COORDINATE SYSTEM

We develop the equations of motion in the noninertial *model* coordinate system, where inertial

torques caused by the Coriolis, the centrifugal, and the angular acceleration (hereafter "spin-up")

forces act on the rotor.   With the prescribed motion of the track, the angular velocity of the

model coordinate system, expressed *in* the model coordinate system is given by

$$\boldsymbol{\omega}_m = [\omega_{m1}, \omega_{m2}, \omega_{m3}]^T = [\dot{\varphi}_T \sin\Delta \sin\theta, \dot{\varphi}_T \cos\theta + \dot{\Delta}, -\dot{\varphi}_T \cos\Delta \sin\theta]^T \qquad (2)$$

The effective body torque $d\boldsymbol{\tau}_{\text{eff}}$ on an element of mass *dm* in the body of the rotor can be written

in terms of the effective body force $d\boldsymbol{F}_{eff}$ using

$$d\boldsymbol{\tau}_{\text{eff}} = \mathbf{r} \times d\mathbf{F}_{\text{eff}} \qquad (3)$$

where

$$d\mathbf{F}_{\text{eff}} = \left[-2\boldsymbol{\omega}_m \times \mathbf{v}_m - \boldsymbol{\omega}_m \times (\boldsymbol{\omega}_m \times \mathbf{r}) - \dot{\boldsymbol{\omega}}_m \times \mathbf{r} + \mathbf{g}\right] dm \qquad (4)$$

r and *v_m* are the position and velocity vectors of rotor mass element *dm*, measured relative to the

model coordinate system. The terms on the right-hand side of the above equation are, in order:

the Coriolis, centrifugal, spin-up, and gravitational forces commonly examined in advanced

undergraduate mechanics courses[5]. All are inertial (i.e. fictitious) except gravity. Integration of

the inertial torque components over all mass elements in the rotor is straightforward, though

laborious, and we omit the details here for brevity. The result is as follows, expressed in the

model coordinate system:

$$\boldsymbol{\tau}_f = \dot{\psi} I_3 \begin{bmatrix} -\dot{\varphi}_T \cos\theta - \dot{\Delta} \\ \dot{\varphi}_T \sin\Delta \sin\theta \\ 0 \end{bmatrix} + \dot{\varphi}_T \Delta I \begin{bmatrix} \cos\Delta \sin\theta (\dot{\varphi}_T \cos\theta + \dot{\Delta}) \\ -\dot{\varphi}_T \sin\Delta \cos\Delta \sin^2\theta \\ 0 \end{bmatrix} + \begin{bmatrix} -(\ddot{\varphi}_T \sin\Delta \sin\theta + \dot{\varphi}_T \dot{\Delta} \cos\Delta \sin\theta) I_o \\ -[\ddot{\varphi}_T \cos\theta + \ddot{\Delta}] I_o \\ (\ddot{\varphi}_T \cos\Delta \sin\theta + \dot{\varphi}_T \dot{\Delta} \sin\Delta \sin\theta) I_3 \end{bmatrix} \tag{5}$$

$$\qquad\qquad \textit{Coriolis} \qquad\qquad\qquad \textit{centrifugal} \qquad\qquad\qquad\qquad \textit{spin-up}$$

where I_0, I_3 and $\Delta I \equiv I_3 - I_0$ are the moments of inertia about the equatorial and polar axes of the

rotor, and their difference, respectively. In the model coordinate system, the torque due to gravity

about the center of mass (coincident with the origin) is zero by symmetry.

IV.   REAL TORQUES IN THE MODEL COORDINATE SYSTEM

In the model coordinate system there are two important pairs of contact forces on the rotor: the

normal forces of contact between axle ends and track, and the kinetic friction forces at those

contacts. To determine their torques, we first use the rotations described in Section II to express

the net gravitational force in the model coordinate system. This gives

$$m\mathbf{g}_m = mg[-\sin\Delta\sin\theta, -\cos\theta, \cos\Delta\sin\theta]^T \tag{6}$$

where m is the mass of the rotor. Gravity acts effectively through the center of mass, which

remains at the origin. The x and z components of $m\mathbf{g}_m$ tend to cause drift of the rotor toward the

edges of the track plane, where they are balanced by normal forces of sliding contact between the

(assumed frictionless) guide ring and the inner edge of the circular hole within which the rotor is confined. Those forces are directed radially inward and generate no torque, but the y_m-component is balanced by the normal forces of contact between the axle ends and the track. Thus,

$$N_- = N_+ + mg\cos\theta \qquad (7)$$

where N_+ and N_- are the magnitudes of the normal forces exerted by the track on the respective ends of the axle.

The net torque on the rotor due to the normal forces is then:

$$\boldsymbol{\tau}_N = \begin{bmatrix} R_T(2N_+ + mg\cos\theta) & 0 & 0 \end{bmatrix}^T \qquad (8)$$

and the torque due to sliding friction forces acting at the locations of the normal forces is

$$\boldsymbol{\tau}_K = \begin{bmatrix} 0 & , \mu R_T(2N_+ + mg\cos\theta)S, & -\mu R_S(2N_+ + mg\cos\theta)S \end{bmatrix}^T \qquad (9)$$

where

$$S \equiv \operatorname{sgn}(\dot\psi - \varsigma\dot\varphi). \qquad (10)$$

$\varsigma \equiv R_T / R_A$ is the track-to-axle radius ratio defined previously, and μ is the coefficient of sliding friction between the axle ends and the tracks. For a given precession rate $\dot\varphi$, Eq.(10), inserted into Eq.(9) embodies the fact that for low spin rate $\dot\psi$, sliding friction acts to accelerate spin and to decelerate the precession. The direction of sliding friction, and the consequent torque, reverses if $\dot\psi > \varsigma\dot\varphi$ since the direction of sliding contact between the axle and the track reverses. Thus the rotor can only accelerate if $S = -1$.

V.   EQUATIONS OF MOTION

The sum of the torques given in (5), (8) and (9) are equated to the rate of change of the angular

momentum relative to the model coordinate system. The resulting equations of motion are

$$\begin{bmatrix} 0 \\ 0 \\ I_3\ddot{\psi} \end{bmatrix} = I_3\dot{\psi}\begin{bmatrix} -\dot{\varphi}_T\cos\theta - \dot{\Delta} \\ \dot{\varphi}_T\sin\theta\sin\Delta \\ 0 \end{bmatrix} + \begin{bmatrix} \Delta I\dot{\varphi}_T\sin\theta\cos\Delta[\dot{\varphi}_T\cos\theta + \dot{\Delta}] \\ -\Delta I\dot{\varphi}_T^2\sin^2\theta\sin\Delta\cos\Delta \\ 0 \end{bmatrix} + \begin{bmatrix} -I_0\sin\theta(\ddot{\varphi}_T\sin\Delta + \dot{\varphi}_T\dot{\Delta}\cos\Delta) \\ -I_0[\ddot{\varphi}_T\cos\theta + \ddot{\Delta}] \\ I_3\sin\theta(\ddot{\varphi}_T\cos\Delta - \dot{\varphi}_T\dot{\Delta}\sin\Delta) \end{bmatrix} + \begin{bmatrix} R_T(2N_+ + mg\cos\theta) \\ 0 \\ 0 \end{bmatrix} + \begin{bmatrix} 0 \\ \mu R_T(2N_+ + mg\cos\theta)S \\ -\mu R_S(2N_+ + mg\cos\theta)S \end{bmatrix}$$

(11,12,13)

| | *Coriolis* | *centrifugal* | *spin-up* | *normal* | *kinetic friction* |

To promote insight into the various terms, we have labeled their sources appropriately. Identical

equations arise if developed in inertial space, with the inertial torques shifted to the left-hand

sides. Because typically $\dot{\psi} \gg \dot{\varphi}$, we now define $\psi_D \equiv \psi/\varsigma$ and cast the equations in terms of

the dependent variables ψ_D and Δ, for which the rates of change are closer in magnitude. We

prescribe $\dot{\varphi}_T$ as constant (steady gyration of the track), we define the dimensionless time

$t_n = \dot{\varphi}_T t$, and *we hereafter express all time derivatives with respect to t_n. Unless otherwise*

stated, all variables from here onward are stated in their dimensionless forms.   Note that the

rotor can steadily accelerate only if (dimensionless) $\dot{\psi}_D < 1$. The dimensionless torque due to the

normal forces becomes:

$$\tilde{N} = R_T(2N_+ + mg\cos\theta)/(I_0\dot{\varphi}_T^2) \tag{14}$$

and Eq. (11) is arranged as an expression for $\tilde{N}$:

$$\tilde{N} = \eta\varsigma\dot{\psi}_D(\dot{\Delta} + \cos\theta) + (1-\eta)\sin\theta\cos\Delta(\dot{\Delta} + \cos\theta) + \dot{\Delta}\sin\theta\cos\Delta \tag{15}$$

where $\eta \equiv I_3/I_0$. Finally, Eqs. (12) and (13) are written as follows:

$$\ddot{\Delta} = (1-\eta)\sin^2\theta \sin\Delta\cos\Delta + \eta\varsigma\dot{\psi}_D \sin\theta\sin\Delta + \mu S\tilde{N} \tag{16}$$

$$\ddot{\psi}_D = -\frac{1}{\varsigma}\dot{\Delta}\sin\theta\sin\Delta - \frac{\mu}{\varsigma^2\eta}\tilde{N}S \tag{17}$$

where Eq. (15) is inserted into the last terms of (16) and (17), and Eq.(10) is written

$$S \equiv \operatorname{sgn}(\dot{\psi}_D - \dot{\Delta} - 1). \tag{18}$$

Eqs. (16) and (17), using (15) for $\tilde{N}$, are coupled differential equations defining the evolution of ψ_D and Δ.

We note here that for the original dynabee, $\varsigma \cong 29$. In the nondimensional Eqs.(16) and (17), reasonable values of $1/\varsigma$ as well as $\sin\theta$ and μ are small. We consider them to be of order $\varepsilon \ll 1$, and keep terms to order unity in Eq.(16), and to order ε in Eq.(17), obtaining the following simplified equations:

$$\ddot{\Delta} - \left(\mu\eta\varsigma\dot{\psi}_D S\right)\dot{\Delta} - \left(\eta\varsigma\dot{\psi}_D \sin\theta\right)\sin\Delta = \mu\eta\varsigma\dot{\psi}_D S\cos\theta \tag{19}$$

$$\ddot{\psi}_D = \frac{-1}{\varsigma}\dot{\Delta}\sin\theta\sin\Delta - \frac{\mu}{\varsigma}S[\dot{\psi}_D(\dot{\Delta} + \cos\theta)] \tag{20}$$

If $S = +1$, Eq.(19) has no stable solution, because the second term behaves as an "accelerative friction", but if $S = -1$ and $\dot{\psi}_D$ is slowly varying, it describes a damped pendulum with a stable equilibrium value near $\Delta \le \pi$. For ease of visualization, we temporarily consider the new variable

$$\gamma \equiv \Delta - \pi \tag{21}$$

so the equations become

$$\ddot{\gamma} + \left(\mu \eta \varsigma \dot{\psi}_D \right) \dot{\gamma} + \left(\eta \varsigma \dot{\psi}_D \sin \theta \right) \sin \gamma = -\left(\mu \eta \varsigma \dot{\psi}_D \cos \theta \right) \qquad (22)$$

$$\ddot{\psi}_D = \frac{1}{\varsigma} \dot{\gamma} \sin \theta \sin \gamma + \frac{\mu}{\varsigma} \dot{\psi}_D (\dot{\gamma} + \cos \theta)]. \qquad (23)$$

If $\dot{\psi}_D < 1$ and slowly varying, the steady-state solution to Eq.(22) is given by

$$\gamma_0 = -\sin^{-1} \alpha \qquad (24)$$

where
$$\alpha \equiv \mu \big/ \tan \theta \qquad (25)$$

Eq.(22) describes a simple damped pendulum, in the presence of a gravity-like torque (proportional to $-\sin \gamma$) and a constant negative torque that deflects its equilibrium from $\gamma = 0$ (hence Eq 24). Eq.(24) also shows that there can be no equilibrium value of γ unless $\mu \leq \tan \theta$. This requirement has been observed by the author[6] . Linearization of Eq.(22) about $\gamma = \gamma_0$ shows that the frequency of small oscillations of the resulting damped harmonic oscillator is

$$\omega_0^2 \equiv \eta \varsigma \dot{\psi}_D \sqrt{\sin^2 \theta - \mu^2 \cos^2 \theta} \qquad (26)$$

and the linear damping coefficient (cf.[5]) of the system is

$$2\beta \equiv \mu \eta \varsigma \dot{\psi}_D \quad . \qquad (27)$$

11

The behavior near equilibrium is underdamped for $\beta < \omega_0$ and overdamped for $\beta > \omega_0$.

Fig.(3a) shows contours of ω_0 and β, as functions of $\dot{\psi}_D$ and µ. A reasonable initial state for the dynabee is shown with a star. Behavior of the system near equilibrium is underdamped, approaching the equilibrium value within a single precession cycle period,

$$\tau_{housing} \equiv 2\pi / \dot{\varphi}_T \text{ (see Fig.3b).}$$

Fig. 3a:Contours of ω_0 (dashed) and β(dotted) for system near equilibrium, for parameters appropriate to the dynabee. θ=15 degrees, η=1.9, ζ=29. Star shows a reasonable value near initial state.

VI.   ACCELERATION OF THE SPIN

When γ is close to equilibrium, Eq.(23) predicts that $\dot{\psi}_D$ increases exponentially, with an e-folding time of

$$\frac{\zeta}{\mu \cos\theta}$$ dimensionless units. This timescale is

roughly two orders of magnitude longer than the variations of Δ, thus validating the requirement that $\dot{\psi}_D$

Fig.3b Numerical integration of Eq.(19) for initial condition indicated in Fig.(3a).

varies slowly. At high rotation rates, it is reasonable to assume that turbulent friction roughly proportional to $\dot{\psi}_D{}^2$ may ultimately limit the acceleration of the spin[7,8,9,10]. Experimental data exist for a rapidly rotating *disk* of radius R immersed in air of density ρ [7,8,9]. The retarding torque is approximated by

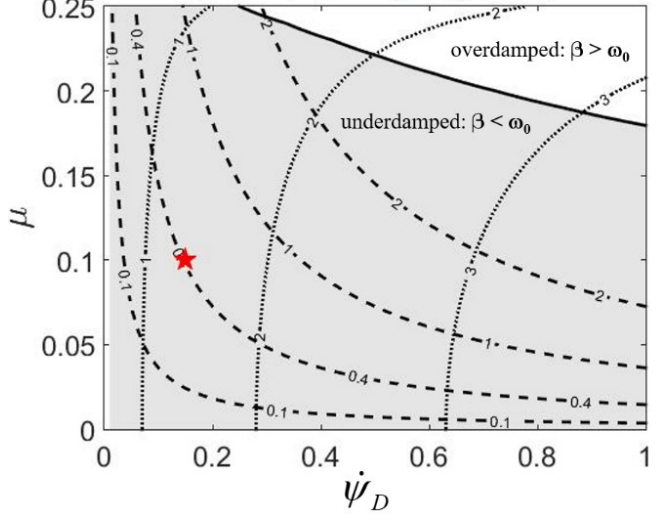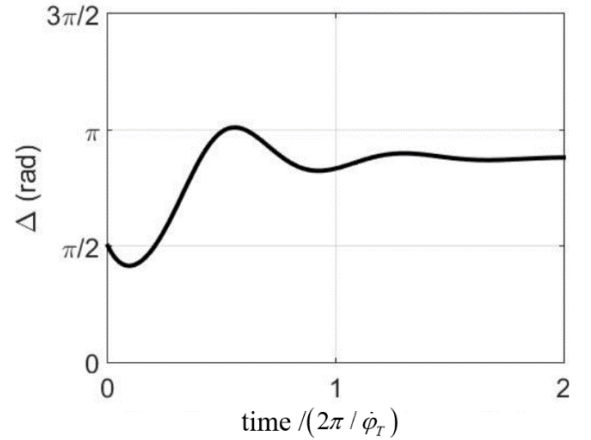$$\tau_{drag} = \tfrac{1}{2} C_m \rho R^5 \dot{\psi}^2 \tag{28}$$

(cf. [8,9]), where C_m is the moment coefficient, which is a function of the effective Reynolds number Re for the system:

$$\mathrm{Re} = R^2\omega \big/ \nu \tag{29}$$

where R is radius, ω is angular speed and ν is the kinematic viscosity of air: $\nu \sim 1.5 \times 10^{-5} \mathrm{m^2/sec}$ [11]. For $\rho = 1.2 \mathrm{kg/m^3}$, a rotation rate of a few x 10Hz, and for R ~2.6cm, corresponding to the original Dynabee, Re $\sim 10^4$,which corresponds to values of $C_m \sim .03$ [9]. Relevant experimental data for a dynabee-like system (partially enclosed housing with spherical rotor) are not known to the author. C_m can only be adequately evaluated by experiment, but geometric considerations suggest that the turbulent friction torque may be considerably larger for a sphere than for a disk, due to the larger surface area with high velocity relative to surrounding air.

With Δ in equilibrium, we write the dimensionless equation of motion for $\dot{\psi}_D$ as:

$$\ddot{\psi}_D = \frac{1}{\tau_D}\dot{\psi}_D\left(1 - \frac{\dot{\psi}_D}{a}\right) \tag{30}$$

where
$$\tau_D \equiv \frac{\varsigma}{\mu\cos\theta} \tag{31}$$

and
$$a \equiv \frac{2\mu I_3\cos\theta}{C_m\rho\varsigma^2 R^5} \tag{32}$$

is a constant describing the characteristic ratio of the accelerating torque, due to sliding friction

at the points of contact, to the torque due to turbulent friction. The solution to Eq.(30) can be

expressed analytically:
$$\dot{\psi}_D = \frac{a \exp\left(\dfrac{t}{\tau_D}\right)\dot{\psi}_{D0}}{\left(\exp\left(\dfrac{t}{\tau_D}\right)-1\right)\dot{\psi}_{D0} + a} \tag{33}$$

For t $\ll$ τ_D, Eq.(33) reduces to

exponential growth, while as t $\rightarrow$

infinity, $\dot{\psi}_D$ approaches a. Fig.4

shows the solution given by Eq.(33),

for a range of values of C_m. If $\dot{\psi}_D$

exceeds unity, the direction of the

sliding friction torque reverses,

reversing the acceleration. Therefore,

these considerations suggest that the

(dimensional) rotational speed of the device

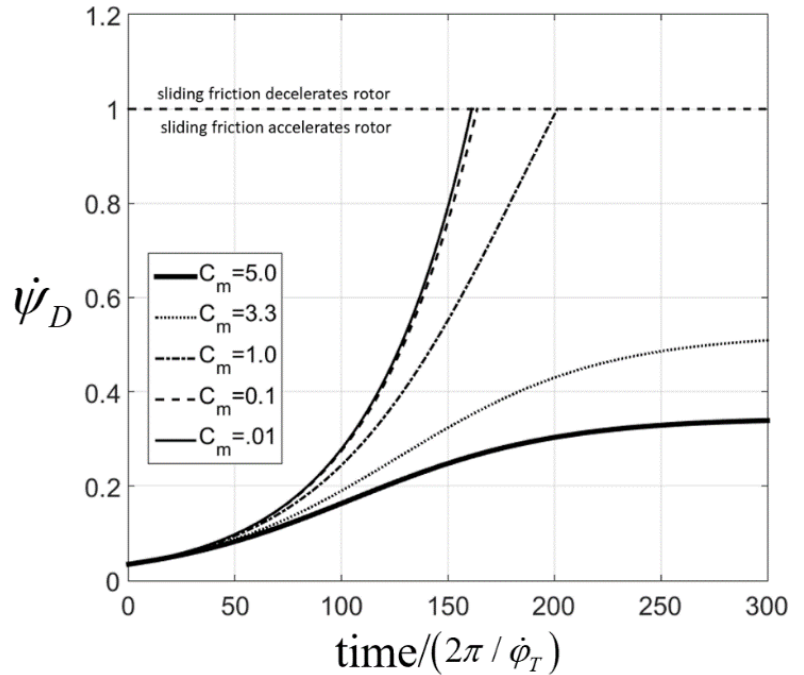should maximize near $\dot{\psi} = \varsigma\dot{\varphi}_T$, never

Fig.4 Evolution of $\dot{\psi}_D$ once resonance is achieved, for various values of the moment coefficient C_m. $\mu=0.1$.

achieving equilibrium between turbulent friction (retarding) and sliding friction (accelerating)

torques. Typically, users of the dynabee gyrate the housing at a maximum frequency of ~2Hz,

indicating that the maximum spin frequency is ~ ςx(2Hz) ~60Hz, agreeing with results of

existing claims of maximum achieved rotation rates [2,3].

VII. TRANSITION FROM SLIDING TO ROLLING

What happens as $\dot{\psi}_D$ reaches 1? At that point, all sliding must stop, and static friction must replace sliding friction. The precise behavior requires a more advanced model of friction than the simple one commonly used in the classroom (which we are tacitly adopting here), where a constant value of sliding friction instantaneously jumps to the higher static value when sliding ceases. The transition from sliding to static friction is an ongoing, complex topic of study[12] that is dependent on numerous factors beyond the scope of this work. In any case, $\dot{\psi}_D$ cannot exceed 1 or the sliding friction would reverse direction, decelerating the rotor. There are potential observables that would indicate that the transition has occurred, if the precise motion of the housing and rotor were to be measured, say, by embedded MEMS motion measurement units (MMUs) in the housing and the rotor . For example, Eqs. (24) and (25) predict a smaller equilibrium value of Δ (larger negative value of γ_0) under static friction. That is, the rotor's +axis should lead the ascending node (section II) by a smaller angle as static friction ensues. Also, in order to maintain resonance, Eq.(25) indicates there would be a larger minimum tilt of the housing for which resonance is possible. The transition from sliding to static friction for the dynabee would be a fascinating subject of future study.

VIII. STARTING THE DEVICE IN THE PRESENCE OF GRAVITY

The presence of gravitational acceleration g imposes a requirement on the minimum axial spin rate $\dot{\psi}$ that allows rotor acceleration. Here the well-known classroom problem of a motorcycle at the peak of a loop-the-loop is conceptually useful. The motorcycle must exceed a critical speed in order to maintain contact with the track when it is at the peak of the loop, upside down. The required speed can be found by requiring the magnitude of the normal force exerted by the track

on the motorcycle to be greater than zero. Similarly in our development, the computed

magnitude of N+ must be greater than zero, if the upper axle end is to remain in contact with the

upper track. If this condition is not met, both ends of the axle will lie against the lower track,

held down by the weight of the rotor. Setting N+ to zero in Eq.(11) gives the minimum spin

frequency:

$$f_\psi = \frac{\dot{\psi}}{2\pi} > \frac{\dot{\psi}_{MIN}}{2\pi} = \frac{R_T g}{4\pi^2 C R_B^2}\left(\frac{2\pi}{\dot{\varphi}_T}\right) = \frac{mgR_T}{4\pi^2 I_3}\left(\frac{2\pi}{\dot{\varphi}_T}\right) \qquad (34)$$

In obtaining (34), we have used the fact that the first term in the Coriolis torque $(-I_3\dot{\psi}\dot{\varphi}_T\cos\theta)$

is larger than all other torque components by a factor of $1/\varepsilon$. The author has observed that the

fastest practical housing gyration frequency for most users is ~2Hz. For the dynabee, Eq.(34)

consequently suggests that the minimum initial spin frequency is ~ 6Hz, which agrees well with

experiments by the author. This corresponds to a value of $\dot{\psi}_D$ of ~0.1. Interestingly there would

be no minimum spin in a zero gravity environment, such as on the International Space Station.

Also the minimum spin for initialization of the desired motion scales inversely as the size of the

rotor, because I_3 is proportional to the radius of the rotor squared, and R_T has a similar value.

Larger devices will require proportionately lower initial spin rates for initialization of the desired

motion.

IX.   TYPICAL OPERATION OF THE DYNABEE

The user of the dynabee initiates the motion by imparting a modest initial spin to the rotor

without tilting the housing. Precession has had no time to develop, so $\dot{\Delta} = \dot{\varphi} - \dot{\varphi}_T = 0 - 1 = -1$.

The initial condition is then $(\dot{\Delta}, \dot{\psi}_D) = (-1, \dot{\psi}_{D0})$ where $\dot{\psi}_{D\min} < \dot{\psi}_{D0} \ll 1$. The user then quickly

tilts the housing, causing opposing axle ends to come in continuous contact with the opposing tracks. The direction of this tilt determines Δ_0, which in turn primarily determines whether resonance is achieved (see next section). An example of a successful initial condition is described by $\Delta_0 = \dfrac{\pi}{2}$, in which case the upper axle end initially lies parallel to the ascending node of the track. The initial tilting action immediately causes precession ($\dot{\varphi}$) to grow, so $\dot{\Delta}$ becomes less negative, while axial spin ($\propto \dot{\psi}_D$) changes much more slowly.

Assuming the user gyrates the housing as prescribed in sections II and III, with an initial axial spin satisfying Eq.(34), resonance is quickly achieved in this case. Fig.(5a) shows the general behavior of the system on the $(\dot{\Delta}, \dot{\psi}_D)$ - plane.

Fig.5a:Sketch of the evolving system on the $\left(\dot{\Delta}, \dot{\psi}_D\right)$ - plane, for successful attainment of resonance.

Fig.5b: Actual trajectory from initial state (star) on $(\dot{\Delta}, \dot{\psi}_D)$ - plane for $\Delta_0 = \pi/2$. $\mu, \eta, \zeta, \dot{\psi}_{D0} = 0.1, 1.9, 29, 0.15.$

Note that the initial conditions place the device in the region above the diagonal boundary (hereafter referred to as the *S-boundary*) prescribed by Eq.(18), where precession accelerates and spin decelerates (S = +1). The rotor cannot begin steady axial acceleration unless the system crosses this boundary, but numerical integration of Eqs.(19) and (20) shows that this happens almost immediately (see Fig.5b), leading to the damped pendulum state (S = -1). While $\dot{\Delta}$
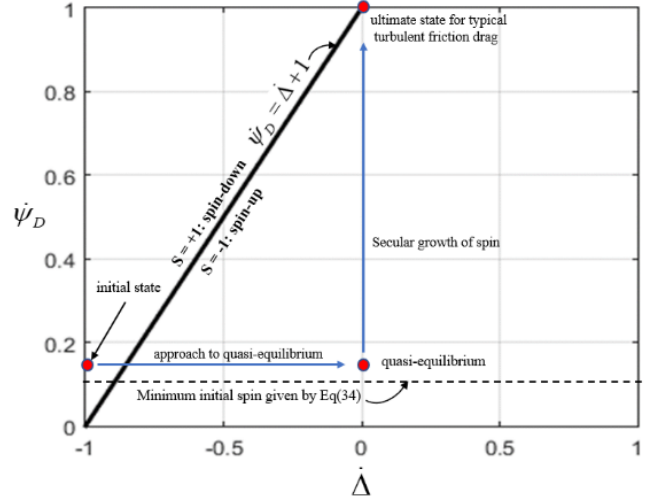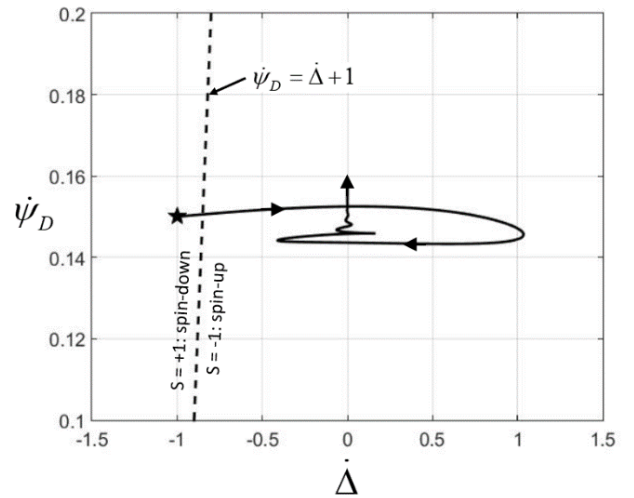
approaches zero, $\dot{\psi}_D$ begins relatively slow secular growth, eventually approaching the

maximum value of unity, where it would cross the S-boundary again if accelerated further. As

mentioned in section VII, static friction may ensue if $\dot{\psi}_D$ reaches unity, but this has not been

verified to the author's knowledge.

X.   ENERGETICS AND RESONANCE CAPTURE FOR THE DYNABEE

We now consider the evolution of the system for all values of Δ_0 between 0 and 2π. Capture of

the dynabee into a resonant state is most easily understood from energetics of the pendulum.

Excluding the term $\propto \dot{\Delta}$, the first integral of Eq.(19) with respect to Δ yields the *effective energy*

E:

$$E = \tfrac{1}{2}\dot{\Delta}^2 + \eta\varsigma\dot{\psi}_D \sin\theta\left(\cos\Delta - S\alpha\Delta\right) \tag{35}$$

The first term on the r.h.s. is an effective kinetic energy, while the rest may be *considered* as

potential energy[13]:

$U(\Delta) \equiv \eta\varsigma\dot{\psi}_D \sin\theta\left(\cos\Delta - S\alpha\Delta\right)$ (36)

For S=-1, $U(\Delta)$ exhibits a series of extrema at

increasing energies as Δ increases, while for

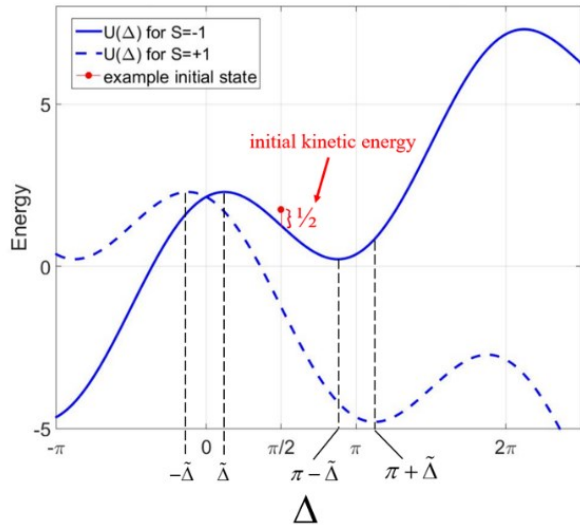S=+1 similar extrema occur with decreasing

successive energies (see Fig.6).

Fig. 6.Potential energy functions for S=-1, S=+1.Example initial state shown. Initial kinetic energy is 1/2 for all states.

Local extrema in $U(\Delta)$, and therefore all

captured states, only exist if $\alpha < 1$, in which case

the first maximum and minimum values of U occur at

18

$$\Delta_{U\,\text{max}} = \tilde{\Delta} \qquad\qquad \Delta_{U\,\text{min}} = \pi - \tilde{\Delta} \qquad\qquad (37\text{a,b})$$

for S=-1, and

$$\Delta_{U\,\text{max}} = -\tilde{\Delta} \qquad\qquad \Delta_{U\,\text{min}} = \pi + \tilde{\Delta} \qquad\qquad (38\text{a,b})$$

for S=+1, where

$$\tilde{\Delta} \equiv \sin^{-1}\alpha \qquad\qquad (39)$$

Since the initial value of $\dot{\Delta} = -1$ (Section IX) the initial value of the kinetic energy is ½ for *all* initial states.

X.1   MODES OF BEHAVIOR

Most generally, the behavior of the system falls into three *modes*, determined entirely by the value of Δ_0. In what follows, we examine the consequences of varying Δ_0 while maintaining the other nominal parameter values assumed in Section IX (see Fig.(5b) caption).

Fig.(7a) shows $E(\Delta)$ for several cases resembling that described in Section IX. Friction quickly drives these states to the local potential minimum at $\Delta = \pi - \tilde{\Delta}$. The system approximates a simple damped pendulum. For $\Delta_0 > \tilde{\Delta}$,   capture occurs if $E(\Delta)$ falls below the maximum at
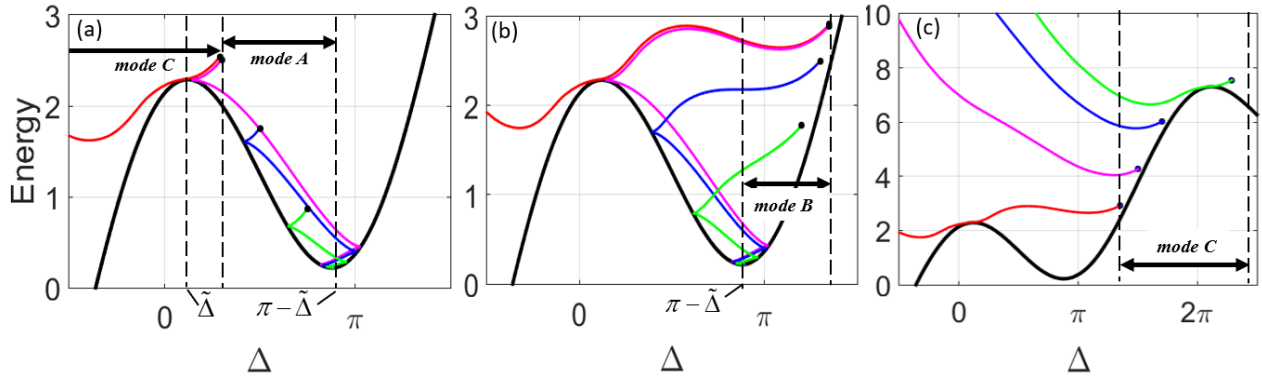

Fig 7:(a), (b), and (c) show E(Δ) for initial conditions corresponding to mode A, mode B, and mode C. See text.

$U(\tilde{\Delta})$ before that point can be reached. We refer to this behavior as **mode A**, and it occurs for a range of values given approximately by $0.29\pi < \Delta_0 < \pi - \tilde{\Delta}$.

Fig.(7b) shows trajectories for values of Δ_0 slightly larger than $\pi - \tilde{\Delta}$. Here the trajectories do not suggest a damped pendulum – most notably for the highest values of Δ_0, where the energy alternately increases and decreases before reaching resonance. We refer to this as **mode B**. For the parameter values assumed here, mode B results when Δ_0 is in the range approximately given by $\pi - \tilde{\Delta} < \Delta_0 < 1.35\pi$. Beyond the upper limit for Δ_0, the system has enough energy to crest the maximum value of U when $\pi = \tilde{\Delta}$. Escape occurs, and Δ diverges toward negative infinity. This behavior, referred to as **mode C**, results for all values of Δ_0 in the approximate range given by $1.35\pi < \Delta_0 < 2.29\pi$, whereafter mode A repeats. Several mode C trajectories are shown in Fig.7c. These modes are most easily understood on the $(\Delta, \dot{\Delta})$ - phase plane. In Fig.(8), trajectories are shown for each mode, against contours of constant *E*. Black dots denote initial conditions for various values of Δ_0, while trajectories for modes A, B, and C are represented by solid, dashed, and dash-dot lines, respectively. The horizontal dashed line is the *S-boundary* given by Eq.(18), for the initial value of $\dot{\psi}_{D0} = 0.15$. Above the boundary, the pendulum is subject to ordinary linear damping (S=-1), approaching the local minimum of *U,* while $\dot{\psi}_D$ slowly accelerates. Below the boundary (S=+1), the pendulum gains energy due to "*negative friction*" -- the accelerative torque proportional to angular velocity $\dot{\Delta}$ (Eq.(19)), while $\dot{\psi}_D$ slowly diminishes. Close examination of Fig.(8) reveals that trajectories indeed spiral "downhill" above the S-boundary, and "uphill" below it.
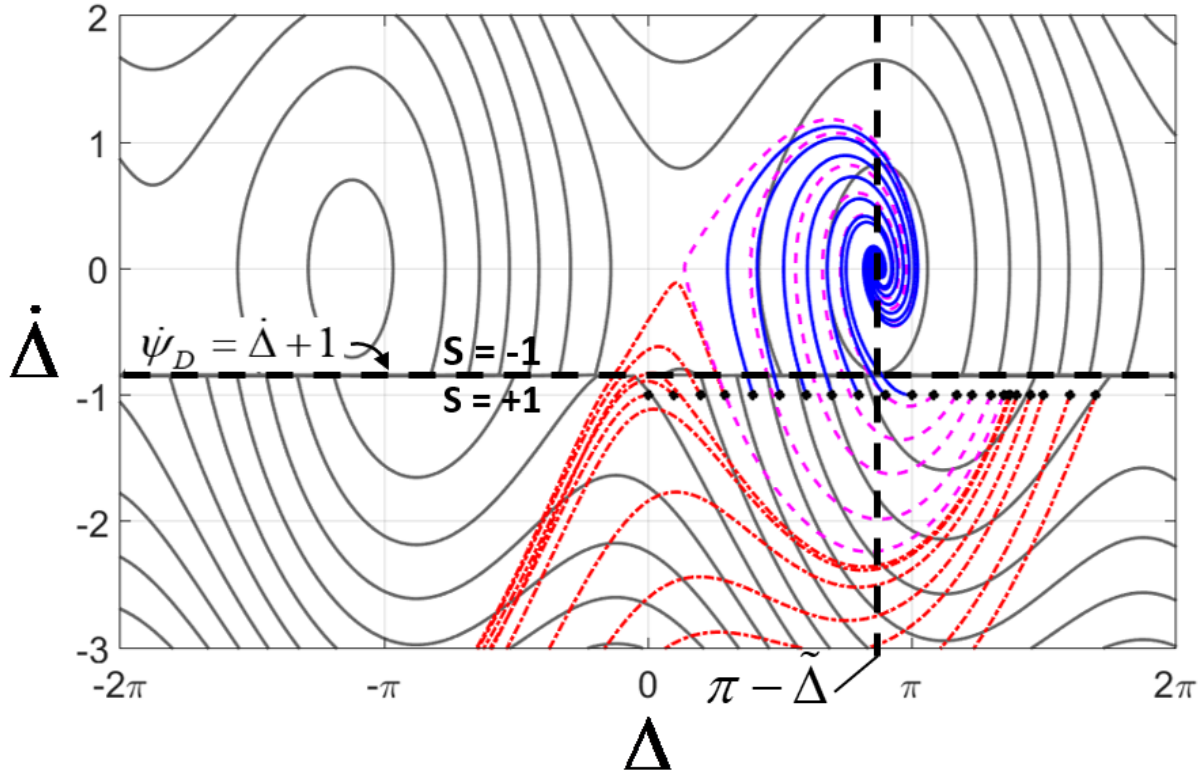
Fig 8: Behavior of dynabee on phase plane. Series of black dots span all possible initial conditions. Mode A (blue/solid), mode B (magenta/dashed) and mode C (red/dash-dot).

Note that the potential energy below the dashed line is unrelated to that above it. The kinetic energy $\frac{1}{2}\dot{\Delta}^2$ remains the same when the boundary is crossed, but the potential energy takes on a new value defined by the contours of U in the newly entered region[14].

All relevant initial conditions lie just inside the region where S=+1. The reason for the simple behavior of mode A is now obvious: standard clockwise motion on the phase plane almost immediately leads these trajectories across the S-boundary, where ordinary damping leads to equilibrium at $\Delta = \pi - \tilde{\Delta}$. For larger values of Δ_0 corresponding to mode B, clockwise motion of the system drives the pendulum deeper into the region where S=+1, and negative friction causes the system to *climb* the energy contours. For mode B, not enough energy is gained to cause escape, and the trajectory eventually crosses the S-boundary into the region of ordinary damping.

The evolution then follows paths identical to those of mode A. Capture has occured, after a slight delay.

For values of Δ_0 corresponding to mode C, the system forays farther below the S-boundary, continuing the clockwise motion on the phase plane while climbing the energy contours due to the negative friction. The system is drawn away from the S-boundary but reverses direction twice, escaping resonance and diverging toward $\Delta = -\infty$. Note that the left-most curves of mode C draw the system into the region of ordinary damping, but once the S-boundary is crossed, the state has crossed the separatrix (not shown) which divides the potential well centered on $\Delta = \pi - \tilde{\Delta}$, from the next lowest well. Subsequent clockwise circulation about that minimum brings the system back below the S-boundary, where negative friction causes Δ to decrease without bound. For all mode C trajectories, negative precession increases at the expense of the axial spin..

XI. CAPTURE PROBABILITY

When a beginner first attempts to operate the dynabee, even after imparting an adequate initial spin, he or she often fails to accelerate the rotor properly, and it stops spinning. The system escapes capture into resonance. What is the likelihood that an unskilled user will achieve resonance when attempting to start the dynabee? There is of course an infinite variety of ways in which an untrained user can fail to accelerate the rotor. However, in the context of this development, we can only assume that our prescribed gyration of the housing is performed (Section II), though not necessarily with successful values of Δ_0. Therefore, we shall assume that after imparting an initial spin, the untrained user of the dynabee will initially tilt the track/housing in a random direction relative to the rotation axis, corresponding to a random value

of Δ_0. As we have seen in Section X.1, only a limited range of Δ_0 values leads to capture. Thus the capture probability is straightforward to compute numerically. It is simply

$$P = \frac{\Delta_{max} - \Delta_{min}}{2\pi} \qquad (40)$$

where Δ_{max} and Δ_{min} are the maximum and minimum values of Δ for which capture occurs. Fig.(9) shows the results of a large ensemble of integrations of Eqs.(19) and (20). Each of the curves was computed for $\mu=0.1$, but with a unique value of $\dot{\psi}_{D0}$ as annotated in the figure. With these values fixed, each
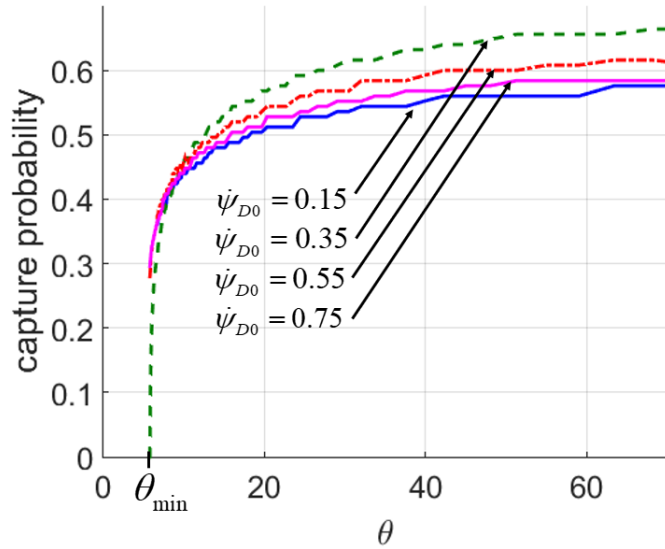

Fig. 9: Capture probabilities for the dynabee. See text.

curve represents 125 values of α in the range $.01 < \alpha < 0.99$. Each value of α corresponds to a unique value of θ, using Eq.(25), where the smallest value of θ for which resonance is possible is $\theta_{min} = \tan^{-1} \alpha \simeq 6^0$. For smaller values of θ, there is no minimum in $U(\Delta)$. Thus it becomes increasingly difficult to start the dynabee successfully as the user employs successively smaller tilts of the housing, even if precessing it perfectly. Consequently, as θ is reduced, P becomes a very strong function of θ. However, P is seen to be a weak function of θ over most of the range shown, ranging from ~50% to ~60% over most values of θ.

Another initially surprising result is that as $\dot{\psi}_{D0}$ is increased above ~0.35, the probability of capture at most values of θ actually diminishes slightly. This is generally contrary to the experience of the user, because with a large initial spin it is easier to perceive the necessary
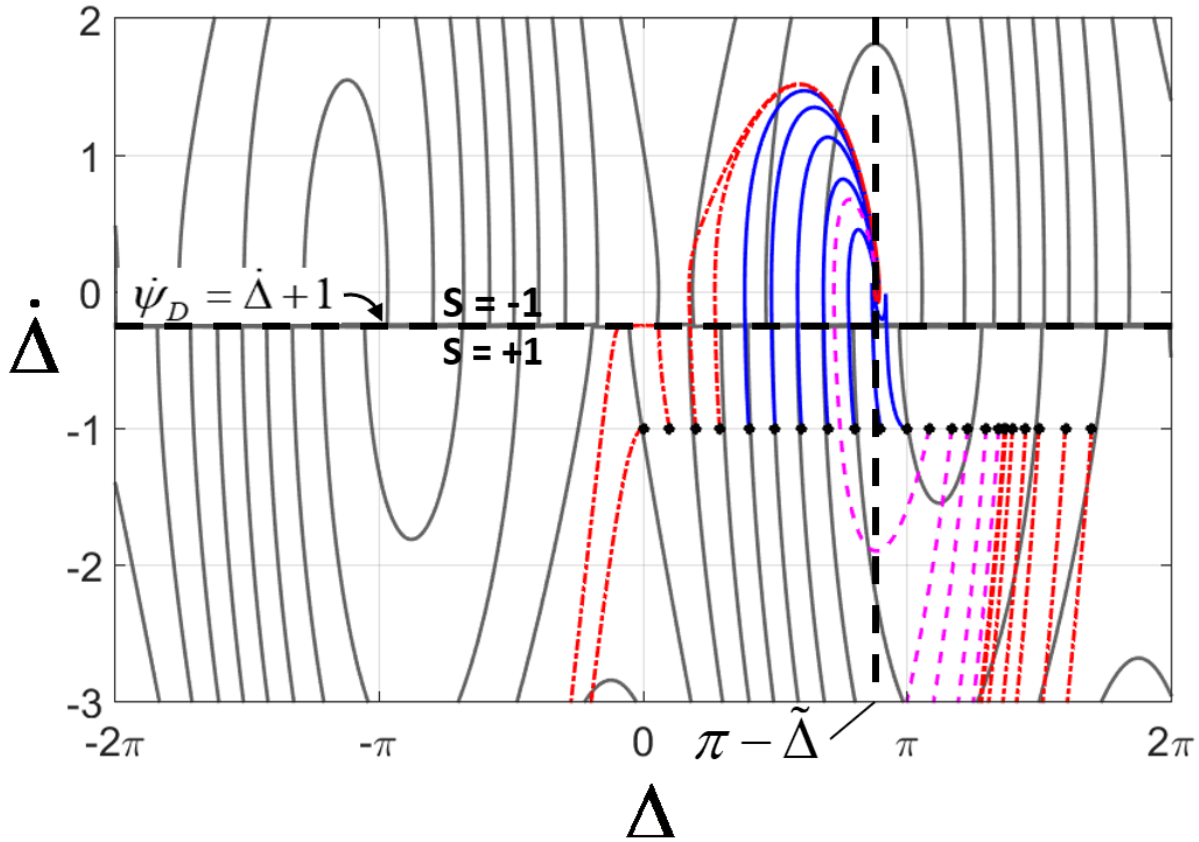
Fig. 10. Phase plane with identical initial conditions as in Fig.8, but with $\dot{\psi}_{D0}$ =0.75. The S-boundary moves upwards, changing the conditions for capture in a subtle manner.

rhythm requited for rotor acceleration. The explanation involves the location of the S-boundary on the phase plane. As $\dot{\psi}_{D0}$ increases, the minima in $U(\Delta)$ become deeper, but simultaneously the S-boundary moves closer to $\dot{\Delta}=0$, and farther from the horizontal line representing initial conditions. For suboptimal choices of Δ_0 leading to mode B, this leads to escape from resonance for an increased range of Δ_0.   Fig.(10) shows the same set of initial conditions as those of Fig(8), but with $\dot{\psi}_{D0}$=0.75. Careful inspection shows that the range of initial conditions giving mode A behavior increases, but the initial conditions giving mode B decreases by a larger amount. The net result is that the probability of escape slightly increases. However, once a user

learns the most effective values of Δ_0 (those of mode A), the probability of mode A capture actually increases with higher initial spin – the dynabee is indeed easier to successfully start.

In general, the above results show that without a skilled choice of initial direction of the tilt (equivalently, a choice of Δ_0), the chances are close to 50/50 that a novice will not successfully start the dynabee's acceleration, even if the track is gyrated as described in section 2, and a good choice of θ is imparted. Having introduced many students to the use of the dynabee, this seems to match the author's experience – students who "get it right" the first time are about as likely as those who require multiple tries before success.

XII.   ANALOGY TO NATURAL SATELLITES IN SYNCHRONOUS ROTATION STATES.

Capture into resonance of the dynabee has a fairly close analog in the tidal evolution of the orbits of nearly all the moons of our solar system, most specifically regarding the nearly ubiquitous phenomenon of *synchronous rotation*, wherein a satellite's average rotational and orbital angular velocities are trapped in a ratio of 1/1. We now examine the similarities between these *spin-orbit resonances* and the motion of the dynabee.

As a moon's spin decelerates due to tidal friction, it typically approaches a state where spin angular velocity only slightly exceeds mean orbital angular velocity (mean motion). In the simplest such state[15], the orientation γ of a natural satellite's minimum axis of inertia relative to the direction toward the primary body, measured at the point of closest approach to the primary body (pericenter), may be modeled as a damped pendulum, as follows:

$$\ddot{\gamma} + \tfrac{3}{2}\left(\tfrac{B-A}{C}\right)n^2\left(1 - \tfrac{5e^2}{2}\right)\sin 2\gamma = \langle T \rangle \tag{41}$$

where *A, B, C, n*, and *e* are the smallest to largest moments of inertia, mean motion, and orbital eccentricity The right-hand side of Eq.(41) is the average tidal torque[16], caused by anelastic response within the body of the satellite to the tidal potential imposed upon it by the primary body. Goldreich and Peale[15] relate this quantity to the MacDonald model of tidal friction[16] within a planetary body near resonance, for which they show that the average tidal torque can be written:

$$\langle T \rangle = -K(V + \dot{\gamma}/n) \tag{42}$$

where *K* and *V* are constants.

With Eq.(42) inserted into Eq.(41), the similarity with Eq.(22) is complete, except for the doubling of the resonant angle in Eq.(41). We note here that in Eq.(22), friction (proportional to μ) is responsible for the same corresponding terms in Eq.(41), and in both cases, the presence of friction is responsible for stability of the resonance.

For the spin-orbit resonance, no stable resonant state can exist unless the maximum gravitational torque due to the primary body acting on the permanent mass asymmetry (proportional to B-A) exceeds the torque due to tidal friction. For the dynabee, the torque due to the Coriolis force in the model coordinate system (see Eq.(12)) plays the role of this gravitational torque, while the terms proportional to μ take the place of the tidal torque.

 A primary qualitative difference between the two phenomena involves the initial conditions. In the case of spin-orbit resonance, the rate of change $\dot{\gamma}$ of the resonant variable is initially positive as resonance is approached, as shown in Fig.(11a,b). Eventually the energy passes a maximum of $U(\gamma)$ for the last time. As $\dot{\gamma}$ decreases to zero due to tidal friction, γ reaches its maximum value.

The kinetic energy vanishes where $E = U(\gamma_{max})$, and the trajectory reverses. If enough energy is lost during .the two-way passage across the potential well, friction leads the trajectory to the bottom of the well. Capture has occurred. Far from the turning point, there is no correlation between the energy and the value of γ at the eventual turning point. In Fig.(11a), a range of trajectories are shown which result in γ_{max} values within the potential well centered near $\gamma \simeq \pi$. The outermost solid curves
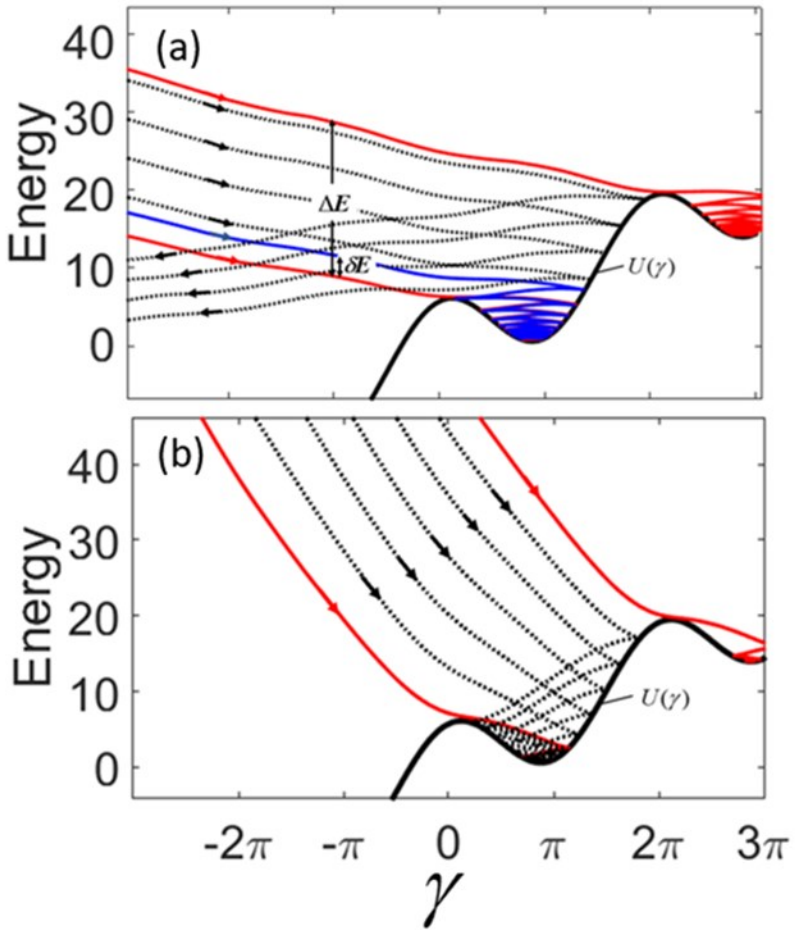

Fig 11a. Fictitious example of approach to spin-orbit resonance. Outer solid curves denote boundaries across which the system enters a neighboring potential well. Range of initial energies for curves within a single well is ΔE. Above the lowest solid curve, the next curve shows beginning of escape. See text.

Fig 11b. Smaller tidal friction. All initial energies lead to capture in this case. See text.

denote the critical trajectories outside of which γ_{max} falls within an adjacent potential well. A range of initial energies δE results in capture. Also shown is the range of energies ΔE outside of which trajectories are duplicated in neighboring potential wells. The capture probability for this fictitiously constructed case is simply

$$P = \frac{\delta E}{\Delta E} \qquad (43)$$

If the system escapes resonance, $\dot{\gamma}$ continues to reduce below zero, meaning that the satellite's spin reduces ever farther below synchroneity with its orbital motion.

In the case shown in Fig.(11b), all initial energies lead to capture. P=1. This case approximates the (simplified) situation for most natural satellites in the solar system, since the great majority are synchronously rotating.

Capture into spin-orbit resonance for planetary bodies is fraught with complexities, some similar to that caused by the dynamical boundary of Eq.(18). For example, as orbital eccentricity is allowed to vary, the direction of tidal torque can reverse. Nonetheless, in a grande réussite, Goldreich and Peale[15] performed extensive theoretical analyses of capture probability analytically for a wide range of planetary bodies. The simple model used to create Fig.(11) is only a fictitious version from which to draw parallels between the dynabee and spin-orbit resonance capture. It is illuminating to note that in spin-orbit phenomena, the small, stable negative value of γ represents the direction of the satellite's long axis relative to the direction of the tide-raising body at pericenter, whereas for the dynabee, γ represents the orientation of the rotor's axle relative to the point of maximum elevation (π/2 ahead of the ascending node). In both cases, the angle would become vanishly small as friction does the same.

XIII.   DISCUSSION AND CONCLUSIONS

Successfully operating a dynabee is a remarkable, visceral experience in the physics and timing of resonance capture. It often brings a look of amazement on the face of a person who has started it successfully for the first time. Yet to those who are skilled at its proper operation, it is hard to imagine *not* operating it successfully. All probability is gone from the experience since the user's central nervous system has learned the proper operation of the device (what is loosely

termed "muscle memory"). For those people, the author recommends trying to start the dynabee with precession in the opposite direction from one's usual direction of precession of the housing. Probability suddenly returns!

Some readers may find it peculiar that a classical, deterministic system can exhibit resonance capture that is probabilistic, but such situations are quite familiar to planetary scientists, as we have seen in Section XII. For spin-orbit resonances, the probabilistic nature comes from randomized initial energy of the pendulum when resonance is approached. When computing capture probability for users of the dynabee, we can only assume that the users do, in fact, gyrate the housing roughly as prescribed in Section II – an assumption that of course is suspect. Under this assumption, however, escape from resonance means the user has chosen a poor initial phase of the gyration – these poor choices are eliminated by practice, so capture is no longer "probabilistic" for the skilled user. Skilled timing of phase eliminates probability.

The results of this work are generally consistent with those of previous authors [2,3], while other results are new. Firstly, our assumption of sliding friction is absolutely essential to any correct model, because the axle immediately slides at initiation of the dynabee's motion, and continues to do so during operation, unless the maximum possible value of spin is reached, where $\dot{\psi} = \zeta\dot{\varphi}$, i.e. $\dot{\psi}_D = 1$. The details of the transition to static friction are complex and beyond the scope of this work. Also, we have shown that in the model coordinate system, the acceleration of the rotor is almost entirely caused, indirectly, by the torque due to the Coriolis force integrated over the body of the rotor. This torque must be balanced by that due to normal forces at the points of contact between rotor and track (see Eq.11), because there is no angular acceleration in the x_m-direction, measured in the model coordinate system. The normal forces in turn are responsible

for the friction torque necessary for acceleration and precession. These details are not immediately obvious!

In this model, the motion of the rotor is driven by the assumed steady gyration of the track, maintained by the user. The user must supply the external torques, due to the normal forces and the sliding friction, described by Eqs (8) and (9), as well as the torques required to gyrate the housing (which we ignore). In the quasi-steady state where $\dot{\Delta} = 0$, combining Eq.(14) and the dominant second term on the r.h.s. of Eq.(15) gives a result for the normal force N$_+$. Inserting into Eqs(8) and (9), the magnitude of the total external torque supplied by the user, expressed in dimensional units, is

$$\tau_{external} = I_3 \dot{\varphi}_T \dot{\psi} \cos\theta \sqrt{1 + \mu^2 \left(1 + 1/\varsigma^2\right)} \simeq I_3 \dot{\varphi}_T \dot{\psi} \cos\theta \tag{44}$$

This result is consistent with [3] if we apply their assumptions of rolling without sliding ($\dot{\psi} = \varsigma\dot{\varphi}_T$). It is stated in [3] that the torque required to operate the dynabee is proportional to the rotation rate squared. Our more general statement is that it is proportional to the product of the precession rate $\dot{\varphi}_T$ and the rotation rate $\dot{\psi}$, which do not maintain a constant ratio as the rotor accelerates. For values appropriate to the dynabee, with a precession rate of $\dot{\varphi}_T / 2\pi \simeq 2Hz$ and the maximum spin frequency of $\dot{\psi} / 2\pi = \varsigma\dot{\varphi}_T / 2\pi \sim 60Hz$, Eq.(44) gives a normal torque magnitude of ~0.5Nm. Dividing by the lever arm for this torque, approximately the radius of the track, gives ~19N or ~4.3lb which is an estimate of the force magnitude applied by the wrist of the user. This agrees with estimates made by the author, and is consistent with the *feel* of the dynabee while it is spinning at a typical high rate. Eq.(44) is also consistent with the torque magnitude derived in [2], using Heyda's method of accelerating the device.

Future research with dynabee-like devices of larger scale may be useful in refinement and verification of friction models near the transition from sliding to *pure* rolling, as the highest possible rotation rate of the rotor is achieved. Such devices would also be ideal as exercise equipment for humans in microgravity environments, since the presence of gravitational acceleration only hinders their operation (see Section VIII) .

Similarities between the motion of the dynabee and celestial mechanics suggest it to be a valuable device for study in advanced mechanics courses. It is rare for a sensate experience like the operation of the dynabee to illustrate such a complex and abstract phenomenon in physics as resonance capture.

---

[*] Department of Chemistry and Physics, Drury University, 900 N Benton Ave, Springfield, MO, 65802
        email: gojakang@drury.edu
[1] Mishler, A. L., 1973, ''Gyroscopic Device,'' U.S. Patent 3726146.

[2] In theoretical mechanics, this is known as a nonholonomic constraint. cf. Lanczos, C, 1970, The Variational Principles of Mechanics, University of Toronto press, Toronto, Canada.
[3] Heyda, P.G.,2001, "Roller ball Dynamics Revisited", *Am. J. Phys* Vol. 70 (10), pp 1049-1051.
[4] Gulick, D.W., and O.M O'Reilly, 2000, "On the Dynamics of the Dynabee", Journal of Applied Mechanics, Vol. 67, pp 321-325.
[5] Marion, J.B, and S. T. Thornton, 1995. Classical mechanics of particles and systems, 4th edition. Thomson Brooks/Cole Publishing, Pacific Grove, CA.
[6] During construction by the author of numerous prototypes of closely related devices, various track substrates were employed. Notably, when contact surface pairs with higher μ -values are used, the device cannot be made to function unless the tilt of the device exceeds a very obvious threshold, felt by the user. With less slippery tracks, the user must tilt the housing at relatively larger values of θ in order to effect capture into the resonant state.
[7] Granville P. S., 1982, "Drag characterization method for arbitrarily rough surfaces by means of rotating disks", J. Fluids Eng. 104 373–7
[8] Vanyo, J.P. , 2015, Rotating Fluids in Engineering and Science, Elsevier Science, NY.
[9]Nelka, J.J., 1973, "Evaluation of a Rotating Disk Apparatus: Drag of a Disk Rotating in a Viscous Fluid", report Accession number AD0766083, Defense Technical Information Center, Corporate Author: David W Taylor Naval Ship Research and Development Center, Bethesda, MD, Ship Performance Dept.
[10]Ovseenko, R.I., Ovseenko, Y.G. (1968). Drag of a rotating sphere. Fluid Dyn 3, 78–82.
[11] "Engineering Toolbox", www.EngineeringToolBox.com
[12] Berger, E.J, 2002, "Friction modeling for dynamic system simulation", Appl Mech Rev, vol 55, no 6.
[13] $U(\Delta)$ is not truly potential energy. The part that is proportional to Δ is actually caused by friction.
[14] This does not violate true conservation of energy because $U(\Delta)$ is not a a true potential energy.
[15] Goldreich, P., and S. Peale, 1966, "Spin-Orbit Coupling in the Solar System", Astronomical Journal, Vol. 71, no.6.
[16] MacDonald, G. J. F, 1964, "Tidal Friction", Rev. Geophys. 2, 467.